Raman scattering from boron-substituted carbon films

J. G. Naeini, B. M. Way, J. R. Dahn, and J. C. Irwin
Department of Physics, Simon Fraser University, Burnaby, British Columbia, Canada V5A 1S6
(Received 12 January 1996; revised manuscript received 7 March 1996)

Raman scattering studies of B_xC_{1-x} films have been carried out for boron concentrations in the range $0 \leqslant x \leqslant 0.17$. The spectra exhibit two broad bands, a graphitic mode (G) centered between 1535 and 1590 cm^{-1} and a disorder-induced mode (D) centered between 1345 and 1370 cm^{-1}. The G mode is observed to soften as a result of boron substitution, and this behavior has been explained using a simple two-dimensional lattice dynamics model. As the boron concentration is increased, a decrease in the intensity of the D band is also observed. Furthermore, the variation of the intensity of the D band with x is found to be correlated with the interplaner spacing. It is thus concluded that the presence of the D mode is associated with the degree of disorder along the c axis. Finally, a phonon confinement model has been used to correlate the linewidth of the G band with the crystallite size in the materials. The results of fitting the calculated line shapes to the measured spectra provides an estimate for the crystallite dimension L_a and also indicates that the frequency and linewidth of the G mode are most strongly influenced by the structural order within the a-b hexagonal planes. [S0163-1829(96)05722-0]

I. INTRODUCTION

It is well known that boron atoms can enter the graphite lattice substitutionally and hence alter some of the physiochemical properties of the original graphite or carbon materials.[1–3] Klein[2] showed that boron doping enhances the electrical conductivity and promotes the graphitization of pyrolytic graphite. A number of groups[3–5] has shown that boron substitution improves the oxidation resistance of carbon materials. A promising application of boron-substituted carbons is in lithium-ion rechargeable batteries,[6] where these compounds may serve as efficient anodes. Traditionally, B_xC_{1-x} had been prepared using high-temperature reaction of B_4C and graphite,[7] with a maximum amount of 2.35% substitutional boron. Recently, there have been reports [8–10] on the synthesis of graphite-structure B_xC_{1-x} solid solutions using low-temperature chemical vapor deposition (CVD) methods, with x as large as 0.25. In particular Way *et al.*[9] have carried out a detailed characterization of a systematic series of carefully prepared samples, using x-ray diffraction (XRD), Auger electron spectroscopy (AES), and x-ray absorption spectroscopy (XAS).

In an attempt to gain additional insight into the structure of these interesting and important compounds we have carried out Raman scattering studies of CVD-grown films,[9] and the results of these experiments are described in this paper. As a result of many previous investigations[11–18] of graphitic carbons, Raman scattering is now widely recognized to be a very powerful technique for the characterization of these materials. In particular, Tuinstra and Koenig[11] reported a Raman line at 1575 cm^{-1} for single-crystal graphite. They also observed the broadening of this line (G mode) and the appearance of additional band at 1355 cm^{-1} (D mode) in disordered carbon materials. Furthermore, they showed that the Raman intensity of the latter band is inversely proportional to the crystallite size in the materials. Subsequently, Nemanich and Solin[12] observed the broadening of the Raman lines by decreasing the size of the graphite microcrystals and attributed this broadening to a relaxation of the conservation of crystal momentum in finite-size crystals.

Further Raman scattering investigations of disordered carbons suggested that the G mode is especially sensitive to the degree of the two-dimensional graphitic ordering,[13] whereas the D mode appeared to be associated with nonplanar microstructural distortions.[14] The results obtained in this paper confirm that the G and D modes are sensitive to the in-plane and c-axis or stacking disorder, respectively, and thus one can use the Raman spectra to delineate between different perturbations. Furthermore, since the present experiments were carried out on samples of known composition, the results obtained can serve as a calibration and this will enable one to obtain an accurate estimate of the boron concentration x from the Raman spectra of B_xC_{1-x} films. Finally, by using a phonon confinement model similar to that introduced by Richter *et al.*[19] and Campbell and Fauchet,[20] we have correlated the Raman spectra of B_xC_{1-x} to the crystallite size in the films and hence have obtained a quantitative estimate for the degree of structural order in the basal plane of these materials.

II. EXPERIMENTAL DETAILS

A. Sample preparation

Thin films of B_xC_{1-x} materials were prepared using a CVD method.[9] By varying the relative proportions of benzene (C_6H_6) and boron trichloride (BCl_3) in a Vactronic CVD-300-M reactor at 900 °C and 5 Torr, thin film samples with $0 \leqslant x \leqslant 0.17$ were attained. The films studied here had thicknesses of about 1 μm and were grown on quartz substrates. The compositions of the films were determined by comparison of their Auger intensities with the signal from B_4C. A Perkin Elmer model 595 scanning Auger microscope was used for these measurements and the systematic errors in the stoichiometries were estimated to be less than 10%. Details of the preparation procedures and AES were described earlier.[9]

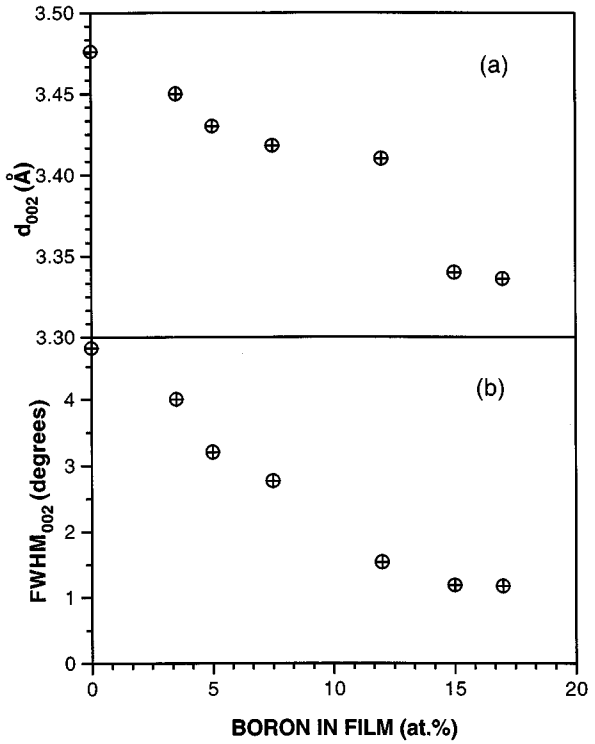

FIG. 1. (a) The d_{002} layer spacing and (b) full width at half maximum (FWHM) of the (002) Bragg peak, both as a function of x in B_xC_{1-x} films.

B. X-ray diffraction

A Siemens D5000 diffractometer with a Cu x-ray tube was used to measure the (002) Bragg reflection of B_xC_{1-x} films. To eliminate the signal from the quartz substrate, a grazing incidence geometry was selected. The results of XRD, which were reported in detail in Ref. 9, are reviewed here for convenience. Figure 1 shows the variation of the interplanar spacing (d_{002}) and the full width at half maximum (FWHM) of the (002) peak as a function of boron concentration. As x increases in the films, d_{002} and the FWHM of the (002) peak decrease. The decrease in d_{002} may be due to the increased graphitization which results from the addition of boron,[2,7] as well as the lower density of the π electrons between the graphite layers because of the fewer electrons in boron. The decreasing FWHM is consistent with the larger c-axis crystallites dimension L_c resulting from the increased graphitization. The $B_{0.17}C_{0.83}$ film has a layer spacing of 3.336 Å which is significantly smaller than for pure graphite, 3.348 Å .[21] This significant interplanar contraction, which is accompanied by further sharpening of the (002) peak, may suggest the formation of an ordered BC_5 compound (near $x=0.17$) having boron atoms arranged regularly within each layer. For lower boron concentration, the boron is thought to be randomly substituted for carbon. A possible atomic arrangement in an ordered BC_5 layer is shown in Fig. 2.

C. Raman scattering

First-order Raman scattering measurements on the B_xC_{1-x} films were carried out using a backscattering geometry. A triple spectrometer with a set of 600 grooves/mm gratings was used for spectral dispersion, which resulted in a spectral bandpass of 800–2000 cm^{-1} and an overall spectral resolution of 4 cm^{-1}. The dispersed light was projected onto a ''Mepsicron'' multichannel imaging detector, allowing data to be acquired simultaneously in all spectral channels. All the spectra were measured at room temperature and the optical excitation was provided by a Spectra Physics 165 Ar-ion laser. We used both the 488 and the 514.5 nm lines to investigate the exciting-wavelength dependence of the spectra. The laser power used was 30 mW and the data acquisition times were typically 2–3 h.

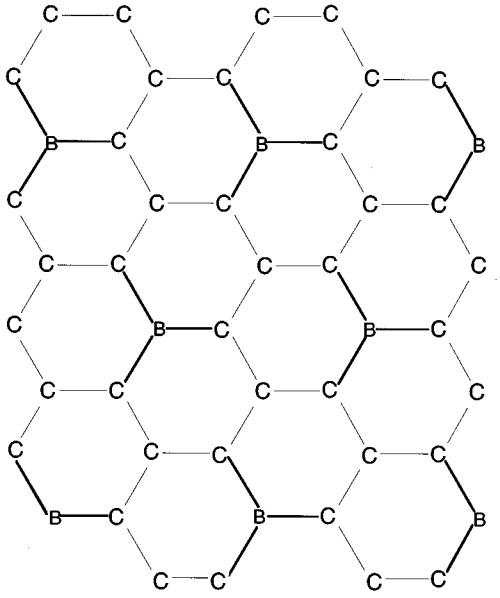

FIG. 2. Possible atomic arrangement in a layer of a BC_5 compound. The C-C and the B-C distances are 1.42 and 1.56 Å, respectively (Ref. 22).

III. THEORY

A. Lattice dynamics model

The Raman spectrum of highly oriented pyrolytic graphite (HOPG) contains peaks at 42 cm^{-1} and 1582 cm^{-1} which have been identified[25] as the zone-center $E_{2g}^{(1)}$ and $E_{2g}^{(2)}$ phonons, respectively. The $E_{2g}^{(1)}$ mode, which corresponds[26] to a rigid layer shearing motion of the interplane van der Waals bonds is very weak and hard to observe.[27] The $E_{2g}^{(2)}$ phonon, on the other hand, corresponds[26] to the stretching of the strong in-plane covalent bonds and therefore exhibits a high frequency. The $E_{2g}^{(2)}$ mode shifts in frequency and broadens significantly (which leads to its designation as the G band) as the material becomes more disordered.[11,12] In addition a new mode (the D mode) appears at about 1355 cm^{-1} and its intensity grows with increasing disorder.[11] The D mode is thought to arise from scattering from zone-boundary phonons which become Raman active because of a loss of translational symmetry.[11] This mode has also been observed[15,17] in B-doped graphite and it has been attributed to symmetry breaking which occurs at boron atoms in the materials.

TABLE I. Material parameters for B and C, obtained from references as indicated.

Physical quantity	Carbon	Boron
Mass (g/mol)	12.01	10.81
Bond length (Å), carbon	1.42[a]	1.56[a]
Bond strength (KJ/mol), carbon	607[b]	448[c]

[a]Reference 22.
[b]Reference 23.
[c]Reference 24.

In an attempt to explain the observed dependence of the $E_{2g}^{(2)}$ frequency on boron concentration in B_xC_{1-x} materials, we have assumed a graphite structure and neglected weak interlayer interactions. To further simplify the model, we assume an ''average'' structure in which a two-dimensional honeycomb lattice is occupied by identical harmonic oscillators of mass m_x and spring constant s_x with an equilibrium separation l_x, given by

$$m_x = m_c(1-0.1x), \tag{1}$$

$$s_x = s_c(1-0.26x), \tag{2}$$

$$l_x = l_c(1+0.1x), \tag{3}$$

where m_c, s_c, and l_c correspond, respectively, to the mass, spring constant, and the spacing of a pure honeycomb carbon lattice ($x=0$). The origin of the above equations becomes more obvious, once we look at the material parameters for B and C, summarized in Table I. For example, the atomic mass of boron is 10 % smaller than the atomic mass of carbon which results in the ''average'' mass m_x given by (1). Similar argument applies for the B-C and C-C bond strength and bond length, which results in Eqs. (2) and (3) for s_x and l_x, respectively.

Figure 3(a) shows a periodic honeycomb B_xC_{1-x} layer with the displacements u and v corresponding to the $E_{2g}^{(2)}$ vibrational mode. The net displacements of the bases with the same indices ($\delta d_{n,n}$) and the bases with different indices ($\delta d_{n,n+1}$), can be calculated using the geometry shown in Fig. 3(b):

$$\delta d_{n,n} = u_n + v_n, \tag{4}$$

$$\delta d_{n,n+1} \approx l_x - d_{n,n+1} = \frac{1}{2}(u_{n+1}+v_n), \tag{5}$$

where in (5) we have assumed u_{n+1} and $v_n \ll l_x$. Using Eqs. (4) and (5) for the net displacements, the harmonic potential energy for a linear chain can be written as

$$U^{\text{harm}} = \frac{s_x}{2}\sum_n (u_n+v_n)^2 + \frac{s_x}{2}\sum_n 2\frac{1}{4}(u_{n+1}+v_n)^2, \tag{6}$$

where the factor of 2, in the second summation, is due to the fact that each basis is bonded to two other bases of different index. Using (6), we solve the equations of motion and thus arrive at the dispersion relation of the $E_{2g}^{(2)}$ optical mode in a periodic B_xC_{1-x} layer:

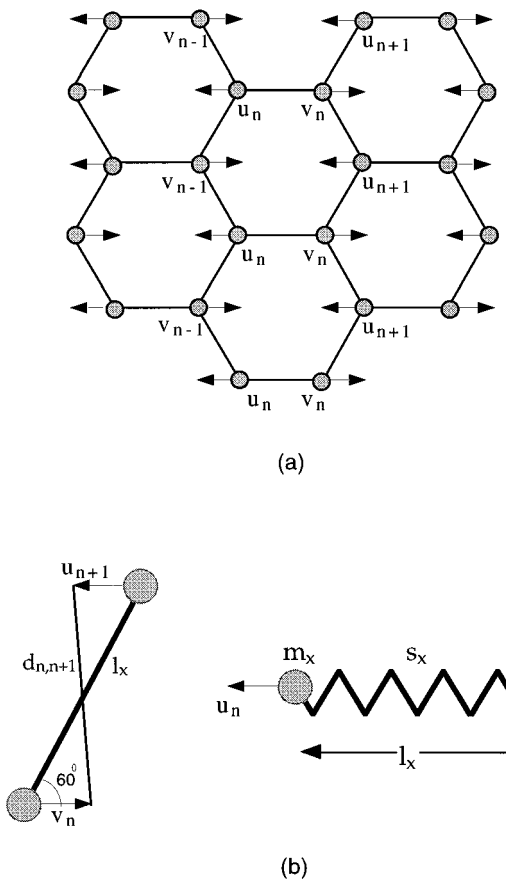

FIG. 3. (a) A periodic honeycomb lattice illustrating the $E_{2g}^{(2)}$ vibrations and (b) the relative displacements of the different bases in the lattice.

$$\omega_x(q) = \sqrt{\frac{s_x}{2m_x}}\sqrt{3+\sqrt{5+4\cos(3ql_x/2)}}, \tag{7}$$

with

$$\omega_x(0) = \sqrt{\frac{3s_c}{m_c}}\sqrt{\frac{1-0.26x}{1-0.10x}}, \tag{8}$$

where in (8) we have used (1) and (2) to substitute for m_x and s_x. The zone-center frequency of a pure carbon lattice, $\omega_c(0)$, is approximately equal to the measured Raman frequency of HOPG:[25]

$$\omega_c(0) = \sqrt{\frac{3s_c}{m_c}} \approx 1582 \ \text{cm}^{-1}. \tag{9}$$

Figure 4 shows the dispersion curves of the $E_{2g}^{(2)}$ mode in pure carbon and $B_{0.17}C_{0.83}$ layers, plotted in the direction of ΓM of the first Brillouin zone (FBZ). The inset shows the FBZ corresponding to a honeycomb lattice. The reduced wave vectors and frequencies are plotted in units of $2\pi/3l_c$ and cm^{-1}, respectively. Upon increasing x in the B_xC_{1-x} layers, the lattice spacing increases, which results in a decrease of the size of the Brillouin zone. This has been indicated by the dashed vertical line in Fig. 4. According to this figure, the frequencies of this branch in a $B_{0.17}C_{0.83}$

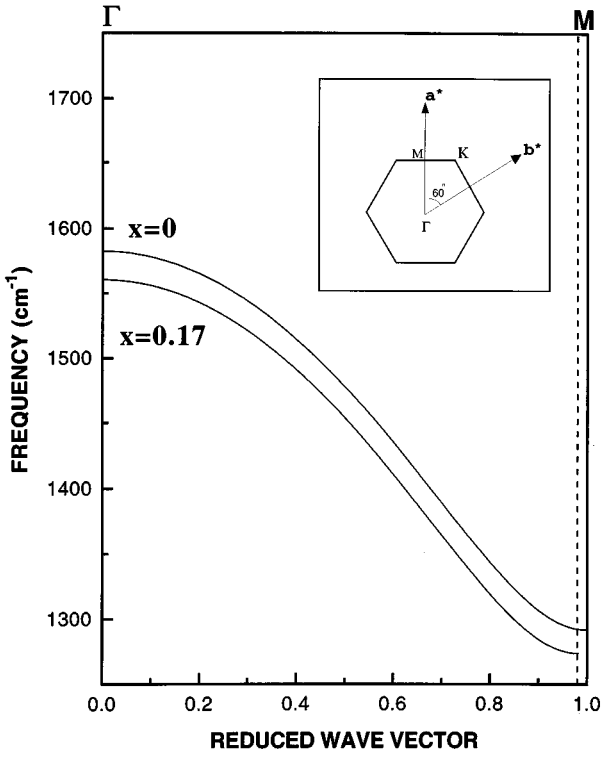

FIG. 4. The calculated dispersion curves of the $E_{2g}^{(2)}$ mode in pure carbon ($x=0$) and $B_{0.17}C_{0.83}$ layers, Eq. (7). The inset shows the first Brillouin zone corresponding to a honeycomb lattice. The reduced wave vectors are in units of $2\pi/3l_c$, with $l_c=1.42$ Å. The vertical dashed line is the zone boundary (M point) in a layer of $B_{0.17}C_{0.83}$.

layer undergo a reduction compared with the frequency of a pure carbon layer (i.e., the mode softens). This can be seen from Eqs. (7) and (8), where the ratio of the spring constant to the mass (s_x/m_x) decreases with increasing boron concentration. In the next section, we will compare (8) with the measured Raman frequencies of the zone-center $E_{2g}^{(2)}$ phonons in the B_xC_{1-x}materials.

B. Phonon confinement model

In 1981, Richter *et al.*[19] formulated a model, now known as the phonon confinement model, which explained the frequency shift and broadening of the first-order Raman spectra of disordered materials. According to this model, in finite-size crystals the $q=0$ momentum selection rule is relaxed and phonons throughout the Brillouin zone contribute to the Raman spectra, with a weight that is determined by the crystallite dimensions. This model was modified by Campbell and Fauchet,[20] to account for the dependence on the crystallite shapes in silicon thin films. Subsequently, the model was used to correlate the Raman spectra to finite-size effects in GaAs alloys,[28] diamond films,[29] polycrystalline silicon doped with boron,[30] and nanocrystalline graphite.[27] We will use this model in an attempt to gain insight into the influence of the crystallite size on the spectral profiles. To begin we assume the presence of cylindrical crystallites with diameter L_a and height L_c. Corresponding to these crystallite dimensions, which might be determined from x-ray diffraction experiments, we introduce correlation lengths

$$\xi=\kappa L_a \tag{10}$$

and

$$\zeta=\kappa' L_c. \tag{11}$$

ξ and ζ will be used in the application of the phonon confinement model and the correlation factors κ and κ' will be determined from a comparison of the Raman results with XRD data. Following the procedures used by Campbell and Fauchet,[20] we construct the Raman line shape corresponding to the $E_{2g}^{(2)}$ mode by superimposing Lorentzian line shapes with linewidth γ centered at $\omega_x(q)$ and weighted by Gaussian functions, i.e.,

$$I_G(\omega,\xi,\zeta)=I'_G(\zeta)\int_0^{2\pi/3l_x} 2\pi q\,dq\,\frac{\exp(-q^2\xi^2)}{[\omega-\omega_x(q)]^2+\gamma^2}. \tag{12}$$

In arriving at (12), we have assumed that (i) the dispersion curves of the $E_{2g}^{(2)}$ phonon in B_xC_{1-x} depend only on the component of the wave vector in the a^*b^* plane and (ii) the FBZ in B_xC_{1-x} is a circle of radius ΓM, which makes the integration over q independent of direction. The dependence of the peak intensity $I'_G(\zeta)$ on ζ is given by[20]

$$I'_G(\zeta)\cong\int_0^{\pi/d_{002}} q'\,dq'\exp(-q'^2\zeta^2)\left|1-\mathrm{erf}\left(\frac{iq'\zeta}{\sqrt{2}}\right)\right|^2, \tag{13}$$

where q' is the component of the wave vector perpendicular to the a^*b^* plane.

IV. RESULTS AND DISCUSSION

Figure 5 shows the first order Raman spectra of B_xC_{1-x} films for $0\leqslant x\leqslant 0.17$, excited by the 488 nm Ar^+ line. The spectra exhibit two broadbands, similar to those observed in disordered and boron-doped carbons.[11–18] These bands have been identified as the $E_{2g}^{(2)}$ or graphitic mode (G), which for $x=0$ is centered near 1590 cm^{-1}, and the disorder-induced mode (D) centered near 1370 cm^{-1}. According to this figure, the frequencies of the G and D bands decrease with increasing boron concentration. Similarly, the intensity of the D band, when compared to the intensity of the G band, decreases with increasing x in the films.

To investigate the laser-wavelength dependence of the spectra we have obtained another set of data using the 514.5 nm line, shown in Fig. 6. According to these spectra, the D band shifts toward lower frequencies (redshift) when compared with the spectra excited by the 488 nm line. A number of groups[16–18] has observed a progressive redshift of the D mode with increasing excitation wavelength, in accordance with our result. Furthermore, we have observed an increase in the D band intensity (relative to the G band) when exciting with the longer laser wavelength. Both Wang *et al.*[17] and Barbarossa *et al.*[18] have reported an enhancement in the D band intensity with increasing laser wavelength, again in accordance with our result.

To obtain an estimate for the D and G band parameters, we fitted the Raman spectra of B_xC_{1-x} films to line shapes of the form

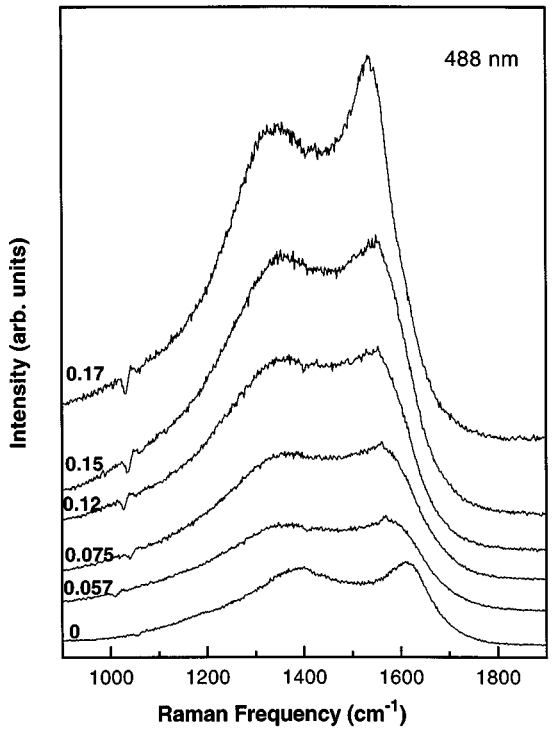

FIG. 5. Raman spectra of the B_xC_{1-x} films excited by the 488 nm Ar^+ line. The boron concentration (x) in the film is indicated on left of each spectrum and the spectra are displaced for clarity.

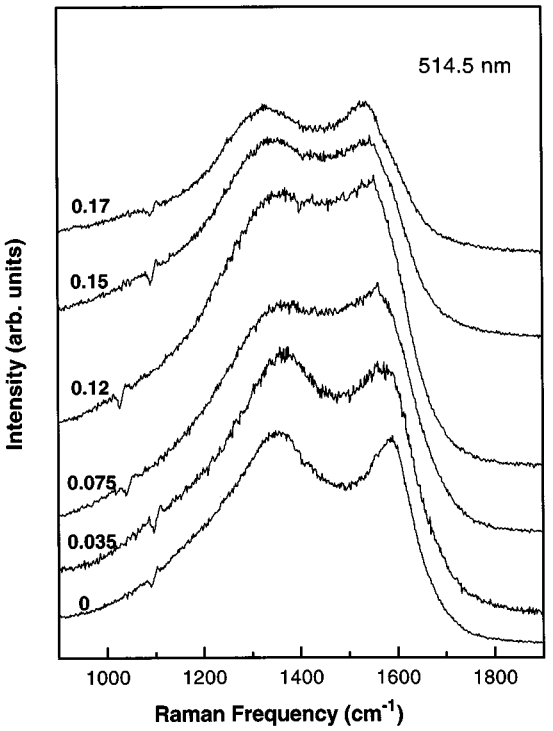

FIG. 6. Raman spectra of the B_xC_{1-x} films excited by the 514.5 nm Ar^+ line. The boron concentration (x) in the film is indicated on left of each spectrum and the spectra are displaced for clarity.

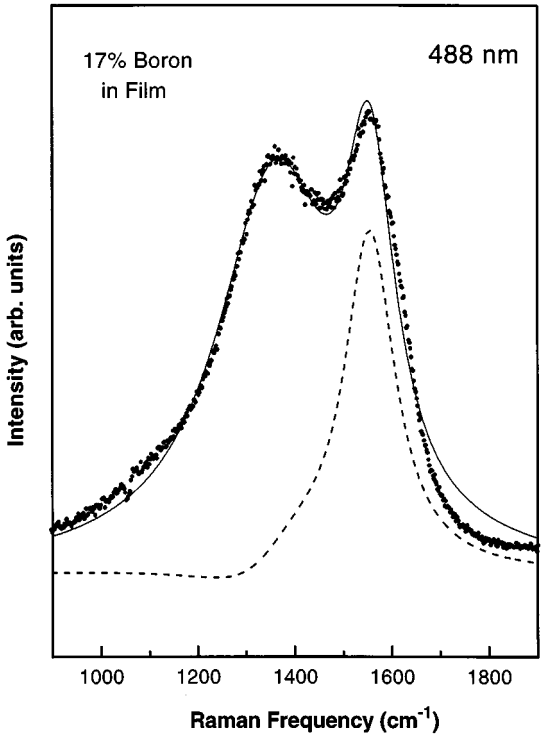

FIG. 7. Fitting Eq. (14) to the Raman spectrum of a $B_{0.17}C_{0.83}$ film. The dashed line is obtained from fitting (12) to the G band. The solid line is the overall fit to the experimental data (dots).

$$I(\omega)=I_0+\frac{I_D}{1+(\omega-\omega_D)^2/\gamma_D^2}+I_G(\omega,\xi,\zeta), \qquad (14)$$

where I_D, ω_D, and γ_D are, respectively, the peak intensity, the peak frequency, and the linewidth of the disordered-induced (D) mode, $I_G(\omega,\xi,\zeta)$ is a line shape which was given by (12) for the G band, and I_0 is a constant background. Figure 7 shows a typical result of fitting (14) to the Raman spectrum of a $B_{0.17}C_{0.83}$ film. The dashed line in the figure is a line shape obtained from fitting the phonon confinement model (12) to the G band.

Figure 8 shows the variation of the Raman frequencies as a function of boron concentration. The solid line in the figure represents the zone-center frequencies of the G mode which have been calculated (8) for single-layer B_xC_{1-x}compounds. The good agreement between the predicted and measured frequencies suggests that Raman spectroscopy can be used to determine the boron concentration in the films. Furthermore, both the measured and calculated trends of the G mode frequencies of B_xC_{1-x} suggest that if the formation of BC_3 ($x=0.25$) is possible, this compound should exhibit a Raman frequency lower than the observed frequency for $B_{0.17}C_{0.83}$ (less than 1550 cm^{-1}). Recently, Fecko *et al.*[10] reported that they had prepared a BC_3 compound and measured a Raman frequency of 1592 cm^{-1} for the G mode in the material, which disagrees with our expectation. In addition, their measured interlayer spacing was ''larger than that of graphite,'' and thus does not agree with the trend of the (002) plane spacing for B_xC_{1-x}, shown in Fig. 1. Since our Raman spectra and XRD results appear to

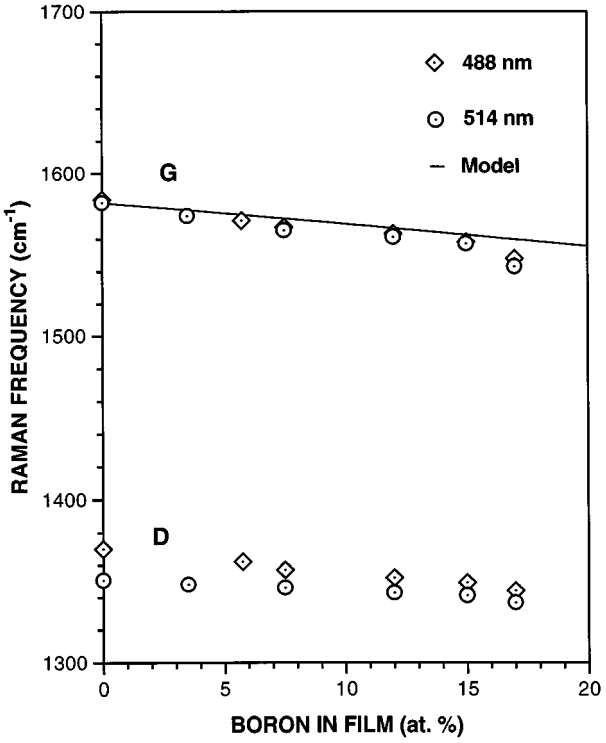

FIG. 8. The dependence of the D and G bands frequencies on x in the films. The solid line represents the results predicted by Eq. (8).

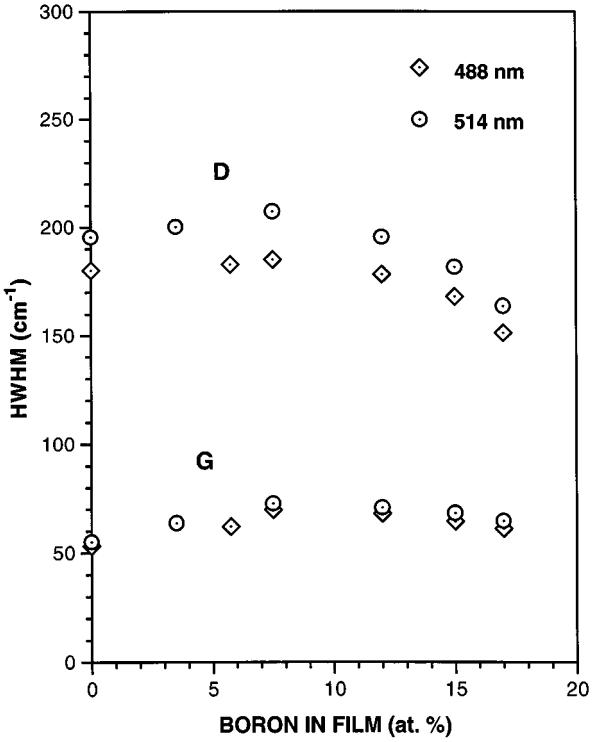

FIG. 9. The dependence of the half width at half maximum (HWHM) of the D and G bands on boron concentration.

establish a clear trend, we suspect that the material prepared by Fecko *et al.*[10] was not BC_3.

Figure 8 also shows the dependence of the Raman frequencies on the exciting wavelength, where the D band undergoes about a 15 cm^{-1} redshift for the longer laser wavelength (514.5 nm). Meanwhile, the G band does not show any significant dependence on the exciting wavelength. This behavior, which is expected[16] for the G mode, suggests that only the G band should be used to determine the basal plane crystallite dimension L_a of the materials.

The variation of the linewidths [half width at half maximum (HWHM)] as a function of boron concentration is shown in Fig. 9. According to this figure, both the bands broaden for $0<x\leqslant 0.075$, presumably due to the random substitution of boron in the films which gives rise to defect scattering and a loss of translational symmetry. However, this trend is reversed in the interval $0.12\leqslant x\leqslant 0.17$ and both the D and G bands are observed to sharpen. This implies increased structural order in the basal plane of the materials which is reflected in the linewidth of the G band, which is most sensitive to the degree of in-plane order.[13] The smallest linewidth for the G band is reached at $x=0.17$, which suggests the formation of a relatively ordered BC_5 phase.

Figure 10 shows the variation of the ratio of integrated intensities (RII) as a function of boron concentration. According to this figure, this ratio decreases with increasing x in the films. Since this behavior is similar to the observed trend in d_{002}, shown in Fig. 1, we might conclude that the D mode is most sensitive to the degree of disorder (graphitization) along the c axis, in accordace with Ref. 14. Furthermore, Fig. 10 clearly shows an increase in the RII for the spectra excited by the longer laser wavelength (514.5 nm). It has been suggested[17,18] that this effect is caused by a resonance enhancement mechanism.

Raman and XRD measurements of $B_{0.12}C_{0.88}$ and $B_{0.17}C_{0.83}$ samples were used to determine the correlation

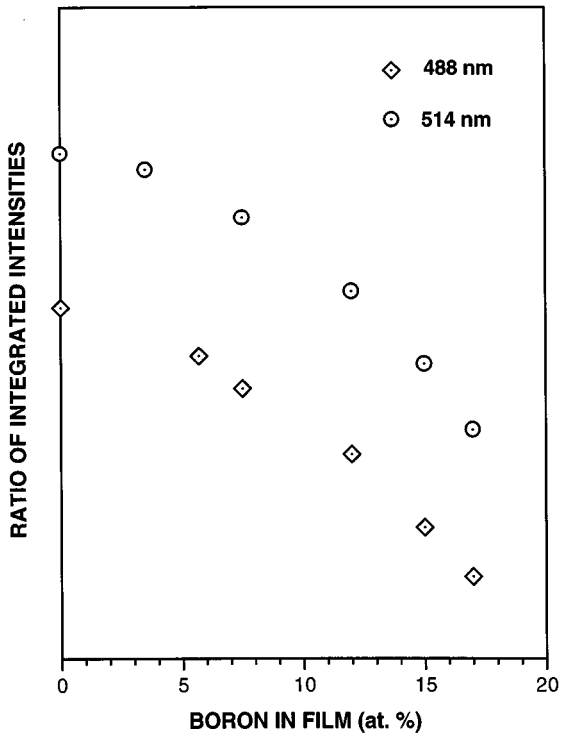

FIG. 10. The dependence of the ratio of the integrated intensities on boron concentration.

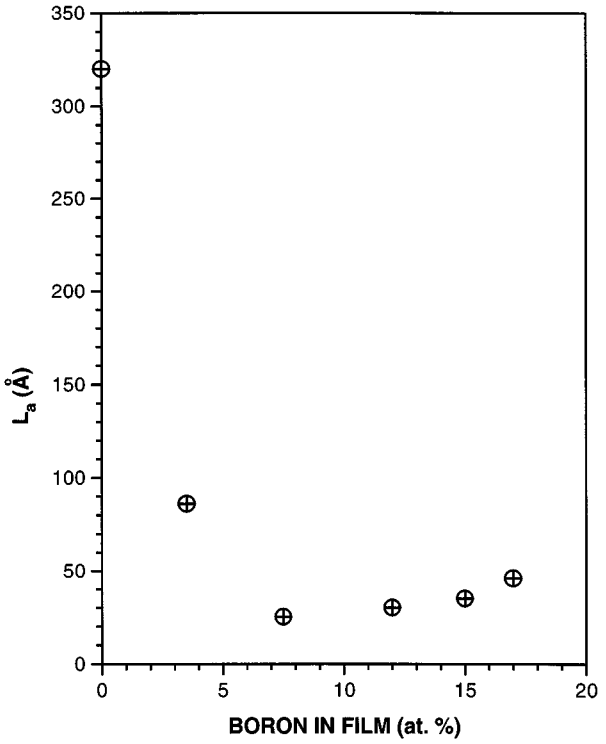

FIG. 11. The dependence of L_a on the boron concentration in the B_xC_{1-x} films.

factor κ, Eq. (10). The fits of (12) to the G mode gave values for ξ which were compared to values of L_a obtained from the (100) Bragg peak of the two B_xC_{1-x} powders. From these comparisons we obtained $\kappa \simeq 1/40$ or $\xi \simeq L_a/40$ for the relation between the correlation length and the crystallite size in the graphite-structure B_xC_{1-x}compounds. Figure 11 shows the variation of L_a as a function of boron in the films. According to this figure, L_a decreases for $0<x<0.12$, but then increases for $0.12 \leqslant x \leqslant 0.17$. The increase in the basal plane crystallite dimension (L_a) for $x \geqslant 0.1$ indicates that the structural order is increasing in this region. This result could be interpreted as being suggestive of the formation of a relatively ordered BC_5 phase ($x=1/6$), consistent with the conclusion reached previously[9] on the basis of XRD measurements (Fig. 1). The different techniques thus yield a consistent picture and this result provides further corroboration of the correlation between the G band and L_a or, equivalently, the dependence of this band on the structural order within basal plane of B_xC_{1-x}.

It should be noted that the values of L_a obtained for samples with $x<0.05$ (Fig. 11) may be much larger than those obtained from XRD measurements. In materials with $x \geqslant 0.05$, the relatively large boron concentration results in relatively small flat crystallites. Thus one should anticipate good agreement between the values of L_a determined from the Raman and x-ray data. In films with $x<0.05$, however, the actual crystallites become more folded and corrugated.[31] In these samples the XRD results provide an estimate of the dimensions of the relatively flat portions of the crystallites. For these same samples, the Raman spectra could provide an estimate of L_a that might approximate better the crystallite dimension, which would thus be much greater than the x-ray result. However, the precise meaning of the Raman-determined L_a is not known in this case. Thus the values of L_a for films with $x<0.05$ must be considered to have greater uncertainties than the values of L_a for films with $x \geqslant 0.05$.

V. CONCLUSIONS

We have carried out a Raman scattering investigation of the vibrational spectra of B_xC_{1-x} for $0 \leqslant x \leqslant 0.17$. As the boron concentration increases from 0 to 0.17, both the $E_{2g}^{(2)}$ phonon (G band) and the disorder-induced mode (D band) soften. Assuming the existence of periodic honeycomb lattices with uniform B_xC_{1-x}bases, we were able to calculate the frequency of the $E_{2g}^{(2)}$ vibrational mode and therefore attribute the mode softening to a decrease in the ratio s_x/m_x of the spring constant to the mass. The ratio of the integrated intensities of the D band to that of the G band decreases as the boron concentration in the films is increased. This behavior is similar to the variation of the d_{002} plane spacing with x, indicating the dependence of the D band on the structural order along the c axis. Furthermore, the D band shows a dependence on the exciting wavelength, in that it undergoes a redshift and an enhancement in the intensity when excited by a longer laser wavelength. Finally we have used a phonon confinement model to correlate the Raman spectra of B_xC_{1-x} films to the crystallite size in the materials. Using the phonon dispersion relation of the $E_{2g}^{(2)}$ mode, calculated for a periodic B_xC_{1-x} layer, we have fitted this model to the G band and hence determined the basal plane correlation length ξ. The correlation length is assumed to be proportional to the basal plane dimension L_a of the crystallites and the constant of proportionality is determined from measurements on samples with $x=0.12$ and 0.17. Both the variation of L_a as a function of boron concentration and the dependence of the G band width on x suggest the attainment of a relatively ordered BC_5 compound near $x=0.17$.

[1] D. E. Soule, *Proceedings of the 5th Conference on Carbon* (Pergamon Press, New York, 1963), Vol. 1, p. 13.
[2] C. A. Klein, in *Chemistry and Physics of Carbon*, edited by P. L. Walker (Dekker, New York, 1966), Vol. 2, p. 225.
[3] J. M. Thomas and C. Roscoe, *Proceedings of the Second Industrial Carbon and Graphite Conference* (Society of Chemical Industry, London, 1965), p. 249.
[4] D. J. Allardice and P. L. Walker, Carbon **8**, 375 (1970).
[5] L. E. Jones and P. A. Thrower, Carbon **29**, 251 (1991).
[6] B. M. Way and J. R. Dahn, J. Electrochem. Soc. **141**, 907 (1994).
[7] C. E. Lowell, J. Am. Ceram. Soc. **50**, 142 (1967).
[8] J. Kouvetakis, R. B. Kaner, M. L. Sattler, and N. Bartlett, J. Chem. Soc. Chem. Commun. **1986**, 1758 (1986).
[9] B.M. Way, J. R. Dahn, T. Tiedje, K. Myrtle, and M. Kasrai, Phys. Rev. B **46**, 1697 (1992).
[10] D. L. Fecko, L. E. Jones, and P. A. Thrower, Carbon **31**, 637 (1993).
[11] F. Tuinstra and J. L. Koenig, J. Chem. Phys. **53**, 1126 (1970).

[12] R. J. Nemanich and S. A. Solin, Phys. Rev. B **20**, 392 (1979).
[13] A. Marchand, P. Lespade, and M. Couzi (unpublished).
[14] T. P. Mernagh, R. P. Cooney, and R. A. Johnson, Carbon **22**, 39 (1984).
[15] T. Hagio, M. Nakamizo, and K. Kobayashi, Carbon **27**, 259 (1989).
[16] R. P. Vidano, D. B. Fischbach, L. J. Willis, and T. M. Loehr, Solid State Commun. **39**, 341 (1981).
[17] Y. Wang, D. C. Alsmeyer, and R. L. McCreery, Chem. Mater. **2**, 557 (1990).
[18] V. Barbarossa, F. Galluzzi, R. Tomacillo, and A. Zanobi, Chem. Phys. Lett. **185**, 53 (1991).
[19] H. Richter, Z. P. Wang, and L. Ley, Solid State Commun. **39**, 625 (1981).
[20] I. H. Campbell and P. M. Fauchet, Solid State Commun. **58**, 739 (1986).
[21] R. W. G. Wyckoff, Crystal Structures (Oxford University Press, London, 1962), Vol. 1, p. 26.
[22] *Tables of Interatomic Distances*, edited by L. E. Sutton (Chemical Society of London, London, 1958).
[23] B. B. Darwent, *Bond Dissociation Energies in Simple Molecules*, Natl. Bur. Stand. (U.S.) Spec. Publ. No. NSRDS-NBS (U.S. GPO, Washington, D.C., 1970).
[24] V. N. Kondratiev, *Bond Dissociation Energies, Ionization Potential, and Electron Affinities* (Mauka Publishing House, Moscow, 1974).
[25] R. J. Nemanich, G. Lucovsky, and S. A. Solin, in *Proceedings of the Intternational Conference on Lattice Dynamics*, Paris, 1975, edited by M. Balkanski (Flammarion, Paris, 1975), p. 619.
[26] K. K. Mani and R. Ramani, Phys. Status Solidi B **61**, 659 (1974).
[27] T. Dallas, M. Holtz, H. Ahn, and M. C. Downer, Phys. Rev. B **49**, 796 (1994).
[28] P. Parayanthal and F. H. Pollak, Phys. Rev. Lett. **52**, 1822 (1984).
[29] J. W. Ager, D. K. Veirs, and G. M. Rosenblatt, Phys. Rev. B **43**, 6491 (1991).
[30] N. Nakano, L. Marvill, and R. Reif, J. Appl. Phys. **72**, 3641 (1992).
[31] R. E. Franklin, Proc. R. Soc. London A **209**, 196 (1951).